CrossMark

ORIGINAL PAPER

Near-Surface Structure of Plasma Polymer Films Affects Surface Behavior in Water and its Interaction with Proteins

Marianne Vandenbossche[1] · Gesine Gunkel-Grabole[2] · Anja Car[2] ·
Laetitia Bernard[3] · Patrick Rupper[1] · Katharina Maniura-Weber[4] ·
Manfred Heuberger[1] · Greta Faccio[4] · Dirk Hegemann[1]

Abstract Using low pressure plasma polymerization, nano-scaled oxygen-rich plasma polymer films (CO) were deposited onto pristine silicon wafers as well as on nitrogen-containing plasma polymer (CN) model surfaces. We investigate the influence of the nature of the substrate as well as a potential sub-surface effect emerging from the buried CO/CN interface, just nanometers below the surface. X-ray Photoelectron Spectroscopy and Time-of-Flight Secondary Ion Mass Spectrometry revealed two important phenomena that occurred during the deposition of the terminal CO layer: (1) a strong degree of oxidation, already for 1 nm nominal thickness, and (2) a gradual transition in chemical composition between the two layers, clearly indicating that effectively a vertical chemical gradient results, even when a two-step coating process was applied. Such terminal gradient film structures were used to study film stability in aqueous environments. Molecular rearrangements were scrutinized in the top-surface in contact with water and we found that the top-surface chemistry and wetting properties of the oxygen-rich termination layer matched those of thick CO reference coatings. Nevertheless, the adsorption of green fluorescent protein (GFP) was observed to be sensitive to the CO terminal layer thickness. Namely, an enhanced protein adsorption was observed for 1–2 nm thick CO layers on CN, whereas a significantly reduced protein adsorption was seen on $\geq$ 3 nm thick CO terminal layers. We

✉ Dirk Hegemann
dirk.hegemann@empa.ch

1 Laboratory of Advanced Fibers, Empa, Swiss Federal Laboratories for Materials Science and Technology, Lerchenfeldstrasse 5, 9014 St. Gallen, Switzerland

2 Department of Chemistry, University of Basel, Mattenstrasse 24a, 4002 Basel, Switzerland

3 Laboratory for Nanoscale Materials Science, Empa, Swiss Federal Laboratories for Materials Science and Technology, Überlandstrasse 129, 8600 Dübendorf, Switzerland

4 Laboratory for Biointerfaces, Empa, Swiss Federal Laboratories for Materials Science and Technology, Lerchenfeldstrasse 5, 9014 St. Gallen, Switzerland

conclude that both, surface and sub-surface conditions significantly affect protein adsorption as opposed to the traditional consideration of surface properties alone.

Introduction

Achieving control over the surface properties of materials widens their range of applications. Amongst the many available surface modification methods, polymer coatings are commonly applied to generate new properties at the surface of materials, such as antifouling [1–3], anti-corrosive [4, 5], bio-sensing [6, 7], heavy metal adsorbent [8, 9] or fire-retardant [10, 11] properties. Homogeneous single-layer coatings are often preferred as they provide a single-step treatment—often by self-assembly. In polymer chemistry, this has led to the design of single precursor molecules carrying multiple functional properties, as in the case of antifouling zwitterionic polymers and peptoids that combine negative and positive charges and assemble into brushes [12, 13]. As an alternative, coating processes based on plasma state processing provide additional benefits for applications in diverse fields, such as (1) a high level of control over the process and free choice of the substrate material, (2) the (covalent) surface treatment of materials without compromising on the bulk properties of the same material [14], (3) the economic use of minimal amounts of substances, and (4) the production of a minimal amount of effluents. Moreover, plasma polymer films (PPFs) are cross-linked and can be characterized by higher stability than conventional polymers [15, 16]. At reduced cross-linking degrees, PPFs can be chemically more functional, but undergo degradation in presence of water [17]. This is an issue in long-term applications in aqueous environments. Indeed, the stability is therefore often antagonistic to its degree of chemical functionality [18–21]. For many applications, a high density of functional groups is essential. Thus, recent studies were carried out to provide stable and sufficiently functional PPFs. These studies mainly consisted in forming a vertical chemical gradient in the plasma coating, by first depositing a cross-linked (and stable) base layer onto the substrate, terminated by a few-nanometer-thick less cross-linked and more functional top-layer [16, 22–24]. This way, functional PPF terminations with enhanced stability were obtained.

Two main methods have been reported in the literature to prepare such PPFs. The first method consisted in tuning the plasma polymerization mode from continuous wave (CW) to pulsed power to provide a vertical gradient regarding chemical composition and cross-linking [24]. Indeed, at comparable power input, the CW plasma polymerization caused stronger fragmentation of the monomers and etching processes, reducing the availability of the desired functional groups, thus leading to more cross-linked polymer-like networks [25]. In contrast, the use of a pulsed plasma polymerization mode reduced fragmentation of monomers and enhanced gas phase radical polymerization during the plasma-off time [26], leading to the retention of a higher level of chemical functional groups [27, 28]. This second method consists of tuning key plasma parameters during the deposition of the film. Indeed, power input, gas flow rates as well as gas flow ratio (for gaseous mixtures, e.g. a monomer mixed with a reactive gas) can be easily changed during plasma deposition [22]. While power input directly affects ion bombardment, which is linked to cross-linking in the PPF, a higher gas flow ratio of reactive gas to monomer gas increases the number of fragments that contain heteroatoms. Accordingly, the number of functional groups in the

coating can increase, yielding less cross-linking in the PPF. Regardless of the method used to provide a coating with a vertical gradient, the sub-surface, i.e. the region underneath the outermost $\sim$ 1 nm thick top-surface termination layer, was observed to have an additional influence on the surface properties, as the gradient coating was found to be more stable than a monolayer entirely consisting of the top layer composition—also when stored in water over days [23]. The precise film architecture, i.e. the thickness of the top-layer, however, might be crucial for the observed stabilization effect.

Only few studies were carried out to investigate the effects of nanometer sub-surface layer of a coating on protein adsorption [27, 29–31], even if it was observed to play a significant role for its properties. A recent study showed that the sub-surface region of PPFs can energetically modify the protein adsorption process [31]. Indeed, adsorption of bovine serum albumin (BSA) protein was investigated on highly stable plasma polymer films, namely a hydrophilic SiO_x, covered by a nanometer-thick hydrophobic layer plasma-polymerized from hexamethyldisiloxane (ppHMDSO) used as terminal coating. If the latter was composed of a 4 nm thick terminal ppHMDSO layer deposited on SiO_x, which was found to significantly reduce protein adsorption on the hydrated gradient structure [31]. As adsorption of proteins onto surfaces involves conformational changes and modified interaction energies in presence of water, studies regarding water penetration into these coatings were carried out [30]. It was observed that water penetrated more than 10 nm into the hydrophobic ppHMDSO within 4 h, while hydration water reached a depth of over 30 nm in the hydrophilic (and nanoporous) SiO_x PPF. It was reported that water molecules in the sub-surface layer can energetically contribute to the protein adsorption process via long-range forces, demonstrating the potential of tailored sub-surface film architecture [31].

The present study aims at investigating the near-surface structure of a nano-scaled oxygen-rich PPF deposited onto a nitrogen-containing base film and its behavior in aqueous media. By varying the thickness of the terminal oxygen-containing PPF, the contribution of the nitrogen-containing sub-surface to the coating properties can be modified and studied. The nitrogen-containing CN film is used in this study as base film and has previously been described and characterized [21]. Likewise, the thicker version of the oxygen-rich PPF has previously been studied, e.g. for biomedical applications [32, 33]. However, the top layer (CO) discussed in those previous studies was 5–10 nm thick, essentially masking a possible contribution from the sub-surface interface. Following our hypothesis that the sub-surface contribution distinctly depends on the top-layer thickness, a series of coatings were here prepared by depositing a 1–3 nm thick oxygen-rich PPF (CO) onto a 5 nm thick base layer of amine-containing PPF (CN). This base layer was carefully analyzed regarding: (1) chemical composition by X-ray Photoelectron Spectroscopy (XPS) and Time-of-Flight Secondary Ion Mass Spectrometry (ToF-SIMS) combined with depth profiling technique; and (2) top-surface properties such as wettability, by water contact angle (WCA) measurements, surface charging, by surface zeta potential (SZP) measurements, and surface interactions via adsorption of green fluorescent protein (GFP).

Methods

Materials

PPFs were deposited onto microscope glass slides (7.6 cm × 2.6 cm) and Si wafers. Substrates were cleaned in an Ar plasma (10 min, 50 W, 10 Pa) prior to plasma deposition. All chemicals were purchased from Sigma Aldrich (Buchs, Switzerland).

Plasma Deposition of the O-rich PPF onto the CN Model Surface

The cylindrical plasma reactor used to perform the PPF deposition consisted of two symmetric plane parallel electrodes (30 cm in diameter) that were separated by a glass ring (5 cm in height). The upper electrode contained a gas showerhead, while the chamber was pumped via a grid through the lower electrode, which was coupled to the RF generator enabling well-defined deposition conditions [34]. A capacitively coupled low pressure discharge with 13.56 MHz radiofrequency excitation was used for the deposition of different PPFs: discharges were carried out in a continuous flow of NH_3/C_2H_4 and CO_2/C_2H_4 mixtures to obtain amine-containing (CN) and carboxylic acid-containing (CO) PPFs, respectively.

As deposition conditions, NH_3 and C_2H_4 flow rates of 7 sccm (gas ratio 1:1), a pressure of 10 Pa, and a power of 50 W was selected to prepare the CN coating [21], while for the CO coating, CO_2 and C_2H_4 flow rates were 24 and 4 sccm, respectively (gas ratio 6:1) at a pressure of 10 Pa and a moderate power of 30 W [22]. Using these conditions reference CO and CN samples, as well as CO/CN coatings (i.e. 1–3 nm CO terminal layers onto CN), were prepared (Fig. 1).

Characterization of the CO/CN Coatings

X-ray Photoelectron Spectroscopy (XPS)

The chemical composition of the surfaces deposited onto Si wafer samples was analyzed by XPS measurements using a Scanning XPS Microprobe (PHI VersaProbe II spectrometer, Physical Electronics) with monochromatic Al Kα radiation (1486.6 eV). The operating pressure of the XPS analysis chamber was below 5×10^{-7} Pa during the measurements. The spectra were collected at photoemission take off angles of 45° (with respect to the sample surface). Survey scan spectra (0–1100 eV) were acquired with an
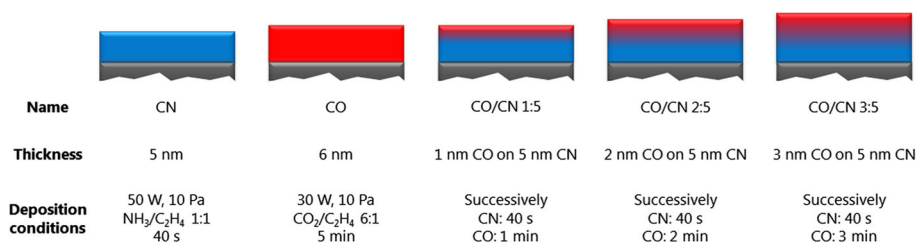

Name	CN	CO	CO/CN 1:5	CO/CN 2:5	CO/CN 3:5
Thickness	5 nm	6 nm	1 nm CO on 5 nm CN	2 nm CO on 5 nm CN	3 nm CO on 5 nm CN
Deposition conditions	50 W, 10 Pa NH₃/C₂H₄ 1:1 40 s	30 W, 10 Pa CO₂/C₂H₄ 6:1 5 min	Successively CN: 40 s CO: 1 min	Successively CN: 40 s CO: 2 min	Successively CN: 40 s CO: 3 min

Fig. 1 Cross-sectional schematic view of the CO/CN coatings developed in this study. Coatings CO and CN denote reference coatings. CO/CN coatings are coatings made of a 5 nm thick CN base layer and different top layers with thickness ranging from 1 to 3 nm

energy step width of 0.8 eV, acquisition time of 160 ms per data point and analyzer pass energies of 187.85 eV. For each sample a randomly chosen spot was analyzed using a micro-focused, scanned X-ray beam with a diameter of 100 μm (operated at a power of 25 W at 15 kV). The 180° spherical capacitor energy analyzer was operated in the fixed analyzer transmission mode (FAT). In order to compensate possible sample charging, dual beam charge neutralization with a flux of low energetic electrons (1.4 eV) combined with very low energy positive Ar-ions (10 eV) was used. Obtained spectra were shifted relatively to the aliphatic carbon (C–C) at 285.0 eV. Curve fitting (least-squares fit routines) with CasaXPS software version 2.3.16 was employed to calculate the atomic concentrations. A mixed Gaussian–Lorentzian product function (constant ratio of 70% Gaussian and 30% Lorentzian) was used to de-convolute the XP spectra and a linear type background was subtracted from the XPS peak areas. For quantification, PHI sensitivity factors [35] were corrected for our system's transmission function and spectrometer geometry (asymmetry function).

Time-of-Flight Secondary Ion Mass Spectrometry (ToF-SIMS) and Depth Profiling

ToF-SIMS measurements (ToF-SIMS.5 instrument, IONTOF, Germany) were performed to analyze the chemical composition of the CO/CN coatings (deposited onto Si wafer pieces of 1×1 cm^2) at the molecular level and more precisely, to identify the molecular composition between the two layers. 50 keV Bi_3^+ primary ions in the high mass resolution mode were used to analyze the PPF topmost surface (first few monolayers) on areas of 100×100 μm^2. To determine the chemical depth profile through the gradient, a layer-by-layer abrasion 250 eV Cs^+ sputtering beam (700×700 μm^2, concentric to the analysis area) was used in combination with Bi_3^+. Note that such low energy sputtering yields a standard in-depth resolution of typically ≤ 2 nm. All negatively charged secondary ions from mass 1–550 atomic mass units were detected in parallel (typical sensitivity in the ppm range) and followed over time while abrading the plasma coating in order to reveal the two layers. After inspection of surface spectra from the reference single-layer samples and assignment of relevant intensity peaks, the following 14 characteristic fragments for both layers and substrate were considered for the analysis of the depth profiles: C_2HO^- (m/z = 41.00), C_3N^- (m/z = 50.01), C_3O^- (m/z = 51.99), $C_3H_2N^-$ (m/z = 52.02), C_3HO^- (m/z = 53.00), $C_3H_3O^-$ (m/z = 55.01), SiO_2^- (m/z = 59.97), C_5N^- (m/z = 74.00), C_6HN^- (m/z = 87.01). All the profiles were calibrated to convert the sputter time into depth (nm), based on independent prediction of the respective layers thickness. For both reference films, CN and CO, as well as for all the CO/CN combinations, three depth profiles have been performed at randomly selected locations to assess reproducibility and film homogeneity.

Water Contact Angle Measurements

Static WCA were determined for two samples (Si wafer pieces of 0.5×2 cm^2) of each coating stored for 30 min in different environments, namely air or distilled water at 20 °C. In addition, the WCA was measured after 1 day of water storage to give a first hint on the stability of the plasma coatings. Samples were then dried by air blowing right before measurements, to remove only superficial water. WCA was measured by depositing at least 3 drops (2 μL) of water (CHROMASOLV®, for HPLC, Sigma Aldrich) onto the surface of each coated sample, and the software controlled drop shape analyser (DSA4, Krüss) was used to determine the contact angle.

Dynamic water contact angles were determined on 3 different samples of each coating after 20 min of air storage. Advancing and receding angles were also measured for freshly prepared PPFs by increasing and then decreasing the volume of the drop. To ensure good and reliable measurements [36] the following protocol was followed using the automatic mode of the DSA25 Krüss device: a drop of 5 μL is first deposited onto the surface—the needle being very close to the surface in the middle of the drop. Then, the volume of the drop was increased to 50 μL at a rate of 30 μL/min and finally decreased until the drop reached a volume of 3 μL. When the drop volume increases, a constant WCA can be obtained after few seconds: this is the advancing WCA. When the drop volume decreases, a constant WCA can also be obtained after few seconds: this is the receding WCA. For each drop, the arithmetic mean of the advancing and of the receding WCA values was reported.

Surface Zeta Potential Measurements

Surface zeta potential (SZP) was measured on coated Si wafers of 3×4 mm^2 size using a Nano ZSP (Malvern Instruments) with a surface zeta potential dip cell (ZEN1020) [37] and the following tracer particles: micromer® PEGylated polystyrene particles [micromod Partikeltechnologie GmbH; monodispersed; size: 1 μm; concentration: 5 μg/mL; at pH: 7.00 ± 0.05 (phosphate buffer)]. The intrinsic zeta potential of the particles is -14 ± 1 mV. As the surface charge has an influence on the mobility of those tracer particles at smaller distance from the surface, the determination of the surface zeta potential was carried out by measuring the velocity of the tracer particles at different distances from the surface (i.e. at 125, 250, 375 and 500 μm). Indeed, close to the surface, the tracer mobility is dominated by electro-osmotic surface flow, which essentially depends on the zeta potential of the surface, and, at larger distances the tracer mobility is dominated by electrophoretic motion; the zeta potential of the tracer particles was thus determined at 1000 μm from the surface of the sample. Surface zeta potential was then calculated from the velocity of standard tracer particles at different distances from the surface of the sample and the known zeta potential of these particles [37].

Atomic Force Microscopy Measurements

Surface roughness of the plasma polymer films (deposited onto Si wafer pieces of 1×1 cm^2) was determined by atomic force microscopy (AFM) just after plasma deposition and after 1 day in distilled water. To perform the AFM analyses, a scanning probe microscope FlexAFM V5 (Nanosurf AG, Liestal, Switzerland) equipped with a C3000 controller and the associated software was used. Areas of 1×1 μm^2 were scanned using a pyramidal silicon tip with a resonance frequency of 190 kHz and a spring constant of 48 N/m (BudgetSensors, Tap190Al-G). Measurements were carried out in tapping mode. AFM images were then analyzed and the RMS roughness was calculated using the open-source software Gwyddion 2.45.

Protein Preparation and Characterization

Recombinant Protein Production

The GFPuv version of the green fluorescent protein (GFP) was used for protein adsorption studies, whereas a yellow fluorescent negatively charged protein (negYFP) was used as reference in zeta potential measurement. Protein negYFP was obtained by site-directed mutagenesis (T214Y) of the negatively supercharged GFP using plasmid pET-6xHis-(-30)GFP. pET-6xHis-(-30)GFP was a gift from David Liu (Addgene plasmid # 62936) [38]. Fluorescent proteins were overexpressed in *E. coli* and purified by immobilized metal affinity chromatography as previously described [39]. *E. coli* BL21 (DE3) chemocompetent cells were transformed with plasmid pPP1 [40, 41]. Cultivations were carried out in LB medium supplemented with 0.1 mg/mL ampicillin and 1 mM IPTG (final concentration), while shaking at 180 rpm. Harvested by centrifugation, cells were lysed by sonication, the cell-free extract clarified by ultracentrifugation, and the His-tagged fluorescent protein separated by affinity chromatography using a Histrap column (column volume = 5 mL) on an ÄKTA Protein Purification Systems (GE Healthcare Life Sciences) using 100 mM potassium phosphate buffer pH 7.00 ± 0.05.

Biochemical Protein Characterization and Zeta Potential in Solution

The purity of the protein preparations and the size of the molecules were determined by SDS PAGE. Absorbance and fluorescence spectra of GFP were recorded in 100 mM potassium phosphate buffer at pH 7.00 ± 0.05. The absorbance and fluorescence properties of GFP were analysed by UV–Vis and fluorescence spectroscopy in 100 mM potassium phosphate pH 7 solutions. GFP concentrations were measured by UV–Vis absorption using a calculated $\varepsilon^{0.1\%}$ of 0.8, at 280 nm. Measurements of zeta potential of the proteins were performed in filtered McIlvaine buffer (Na_2HPO_4, citric acid) in a pH range from 2.2 to 8 using a Malvern Zetasizer at 25 °C.

Protein Structure Analyses

The software Pymol [42] (The PyMOL Molecular Graphics System, Version 1.7.4 Schrödinger, LLC) was used to visualize the three-dimensional structure of GFP (PBS ID: 1eme) as retrieved from the Protein Database [43]. Surface potential was visualized using the Adaptive Poisson-Boltzmann Solver (APBS) using default charge values and a solvent dielectric constant of 80 (water at pH 7) [44].

Protein Adsorption onto the CO/CN Coatings

Visual analysis of Protein Adsorption

Before treatment, plasma-treated surfaces deposited on glass slides were incubated overnight in deionized water to neutralize the still-living radicals [45, 46]. Protein adsorption was assessed by depositing 200 μL of a solution containing the green fluorescent protein, GFP in 100 mM potassium phosphate pH 7.00 ± 0.05 at a protein concentration of 2 mg/ml onto the coated surfaces and incubated at 22 °C for 30 min in the dark under moist conditions. Samples were then rinsed for 2 min in distilled water (3 times) before they

were gently dried in air, while covered by aluminum foil, before characterization. Samples were prepared in triplicate to ensure repeatability.

Imaging of Adsorbed Proteins on the Coatings

Surfaces treated with GFP were imaged with a LS Reloaded Microarray Scanner (Tecan, Switzerland) using a 488 nm laser, a FITC filter (535 nm), a 140 gain, and a 10 μm resolution with a small pinhole. Images were then analyzed with the software provided by Tecan (Switzerland) to determine the fluorescence intensity averaged over a grid of nine circles (Ø = 2 mm). Fluorescence intensity values obtained from surfaces incubated with protein-free buffer solutions under identical conditions of temperature and time were used as control and subtracted from the values obtained.

Results and Discussion

A base CN coating was initially prepared as reference model surface with a nominal thickness of 5 nm to ensure highly stable, amine-functional plasma polymer films [21]. The CO reference coating was deposited onto pristine (and plasma-cleaned) Si wafers with a nominal film thickness of 6 nm, to ensure full coverage of the substrate. In addition, the CO film of variable thickness (1–3 nm) was deposited onto 5 nm of CN according to a sequential process. For all CO/CN coatings, the nominal thickness values of the terminal layer were based on the previously determined deposition rate of the plain plasma polymer film (i.e. CO reference), at a rate of $\sim$ 1.2 nm/min for CO. As plasma polymerization occurs through both deposition and etching processes, a mixture of nitrogen- and oxygen-containing chemical groups may form at the interface between the two layers leading to a vertical chemical nano-gradient through the nano-film. Moreover, with a thickness of the top-layer of about 1–2 nm, chemical groups from the CN layer are expected to have an influence on surface properties, i.e. the chemical gradient layer might extend to the outermost surface.

Characterization of O-rich PPF Deposited onto CN Model Surface

After deposition of the PPFs, representative samples were analyzed by XPS to determine their chemical composition (Fig. 2a). At a take-off angle of 45° only approximately 6 nm of the coating is analyzed due to exponentially decreasing information content gained from the depth, and thus, the analyses refer to the upper PPF layer as well as the base layer of the coatings CO/CN. No nitrogen was detected in the plain CO whereas around 8 at% of oxygen were observed in the plain CN coating (in addition to 14 at% of [N]). Moreover, a slight amount of Si was observed in the CN coating. Due to the PPF thickness examined and the information depth of XPS, the silicon signal and part of the oxygen signal originated from the SiO_2 layer terminating the Si wafer. Yet, some of the oxygen signal also stems from the CN layers, which is even seen for thicker coatings [21]. Thus, presence of oxygen in the CN layer might be due to (1) few ppm of oxygen (residual gas) in the plasma chamber even if the plasma deposition is carried out at low pressure, or due to (2) the presence of long-living radicals trapped in the PPF reacting with atmospheric oxygen after the deposition process (post-ambient plasma oxidation). According to XPS analyses the amount of heteroatoms was relatively similar for all prepared samples (see Table S1,
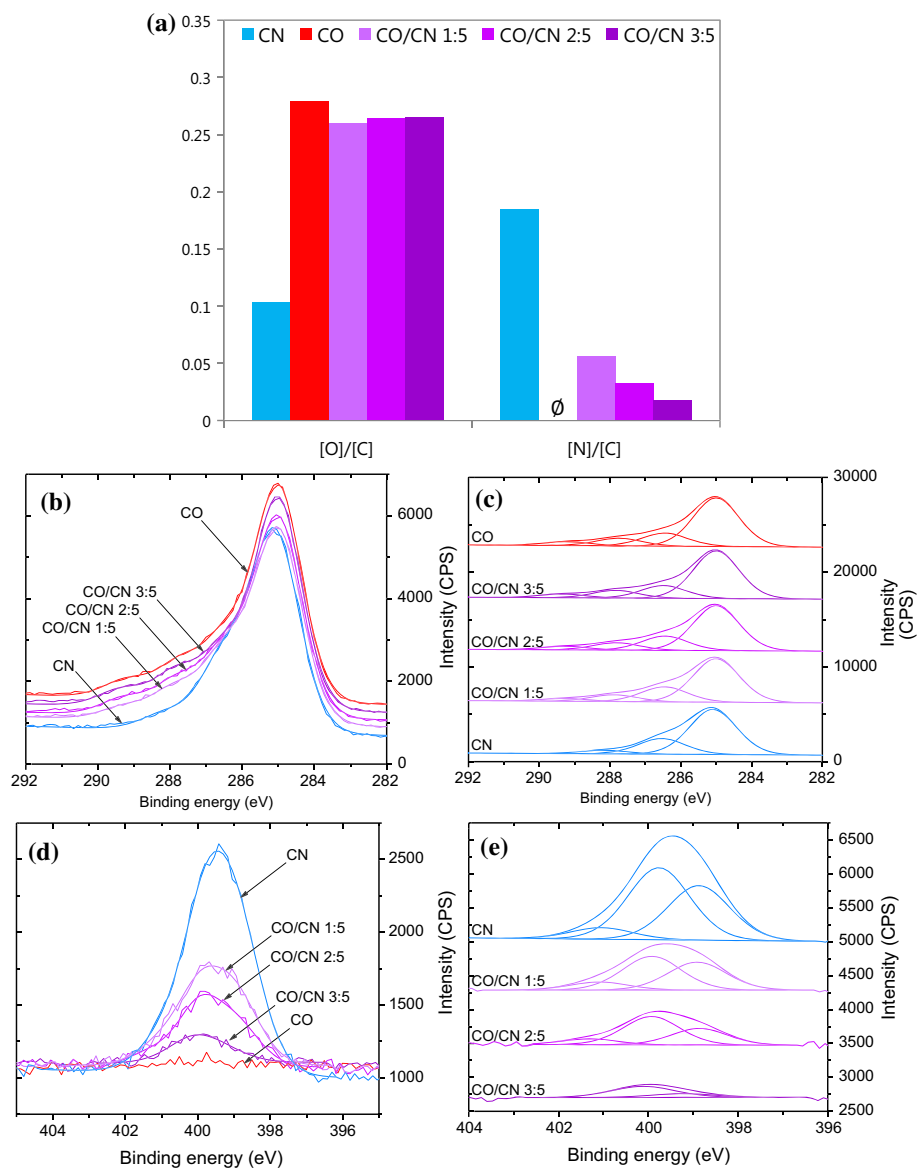
Fig. 2 Comparison of **a** [O]/[C] and [N]/[C] ratios calculated from X-ray Photoelectron Spectroscopy (XPS) region data, **b** high resolution C1s peak and **c** de-convoluted C1s peak, **d** high resolution N1s peak and **e** de-convoluted N1s peak from XPS spectra analysis of the CN, CO and CO/CN (1:5, 2:5, 3:5) coatings

supplementary information), and slightly higher for the CO/CN 1:5 and 2:5. However, the amount of oxygen and nitrogen was clearly different for CO and CN (Fig. 2a).

A similar [O]/[C] ratio, i.e. around 25–27%, is observed for the coatings CO and CO/CN (independent of the thickness of the CO top-layer on the CN layer), whereas lower [O]/[C] ratios were obtained for the CN coatings of around 10.3%. Regarding the [N]/[C] ratios, the same trend can be noticed. Indeed, from XPS analyses, no nitrogen content is

detected in the CO coating. Furthermore, a decreased amount of nitrogen was observed with the increase of the terminal CO layer thickness: [N]/[C] ratio was 5.6, 3.3, and 1.8% for a CO layer thickness of 1, 2, and 3 nm, respectively. As expected, the CN coating contained a higher amount of nitrogen ([N]/[C] = 18.5%). Since the top 6 nm were analyzed by XPS under these experimental conditions, both the top layer and the base layer contributed to the measurement of the chemical composition, also involving the entire chemical gradient.

Evidence for added oxidation of the CN layer, i.e. formation of a vertical chemical gradient, can be given by considering the detail spectra of C1s and N1s (Fig. 2b, d). Indeed, the C1s photoelectron signal peaks (Fig. 2b, c) are broader, indicating the presence of an additional oxidation state, since a layer of CO (> 1 nm) was deposited onto the CN layer. This can also be supported by the finding that C1s peaks of CO and CO/CN coatings were best de-convoluted with 4 peaks, whereas 3 peaks were adequate to de-convolute the C1s peak of the CN coating alone. As one might expect, a clear decrease of the nitrogen content was observed by increasing the thickness of the CO layer on top of the CN base layer (Fig. 2d, e). The [N]/[C] ratio decreased from 18.5 to 5.6% by adding 1 nm of CO onto the CN layer (CO/CN 1:5), whereas it decreased further from 5.6 to 3.25% and from 3.25 to 1.80% by increasing the CO layer thickness to 2 and 3 nm (CO/CN 2:5 and CO/CN 3:5), respectively (Fig. 2a, d). Thus, a significant oxidation of the interface with the CN layer occurred during the deposition of the first 1 nm of terminal CO induced by the high CO_2/C_2H_4 gas ratio used yielding chemical (oxidative) etching. For thicker CO/CN coatings, the decrease of N1s peak corresponds to the expected signal attenuation of photoelectrons across a thicker CO top-layer.

ToF-SIMS depth profiling chemical analyses were carried out on CN, CO reference and CO/CN double layer coatings, to assess the molecular composition of these coatings. Thereby, the chemical composition as a function of the depth in the coating of the CO layer deposited onto either the CN base layer or the Si wafer can be compared. Figure 3 shows the in-depth evolution of selected characteristic nitrogen- and oxygen-containing fragments, i.e. C_3N^- (Fig. 3a) and C_3HO^- (Fig. 3b).

As observed on Fig. 3a for the fragments C_3N^-, the intensities of the nitrogen-containing fragments were higher for the CN layer than for the CO coating. Moreover, CO/CN
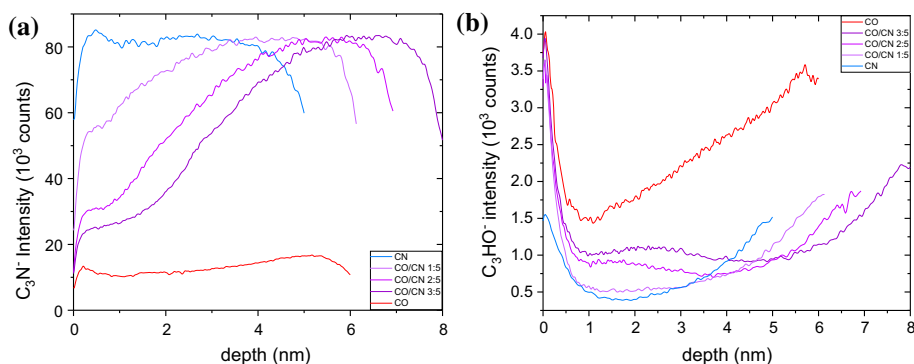

Fig. 3 Depth profiles obtained by Time-of-Flight Secondary Ion Mass Spectrometry (ToF-SIMS) for the three CO/CN 1:5, 2:5, and 3:5 structures, respectively, compared to the references CN and CO. Intensities of the nitrogen-containing fragments, i.e. C_3N^- (**a**), as well as intensity of the oxygen-containing fragment, C_3HO^- (**b**), are given as a function of the depth (where 0 corresponds to the outer surface)

coatings exhibited a gradual transition (over a range of approximately 2 nm) between the top-layer CO and the base layer CN (at different depth according to the thickness of the CO layer), even if double layer coatings were produced by a subsequent (two-step) process. Thus, formation of a vertical chemical gradient occurred during the coating process. The formation of the gradient structure is likely due to the fact that the terminal layer deposition, i.e. the CO layer, was prepared under plasma conditions that promote moderate chemical etching of the underlying CN layer. The used gas flow ratio CO_2/C_2H_4 of 6:1 is known to enhance etching phenomena during plasma deposition [47, 48]. Consequently, at the early stage of deposition of the terminal CO layer, (ion-assisted) oxygen etching occurs, yielding oxidation and formation of radical sites as well the release of some nitrogen-containing species into the plasma zone. These species are able to react with other species in the plasma zone and can also be re-deposited onto the surface, leading—together with the oxidation processes—to the formation of a vertical chemical gradient.

According to expectations, the oxygen-containing fragment C_3HO^- was counted higher or lower from the pure CO or CN coatings, respectively. Anyway, the evolution of the intensity of the C_3HO^- fragments (Fig. 3b) in the depth of the CO and CN reference coatings followed the same tendency: (1) an important decrease of the intensity counts occurs in the first 0.5 nm of both coatings, and is followed by (2) a regular increase of the intensity counts until the PPF/substrate interface is reached. The first 0.5 nm actually corresponds to the oxidation layer at the extreme surface of all coatings (< 1 nm thick), and is formed due to post-plasma oxidation process. The increase in intensity observed close to the interface between the PPF layer and the Si wafer is actually due to a so-called matrix effect (the proximity of the oxygen from the substrate promotes the ionization potential of secondary ions) in addition to a possible recombination of some substrate oxygen atoms with polymer fragments. As coatings have very small thicknesses in this study, these effects hinder the precise behavior of the oxygen-containing fragments in the depth of the coatings. Anyway, differences in between the CO/CN coatings can be observed on Fig. 3b. Indeed, higher intensity count values were found at the top surface, highlighting the post-plasma oxidation process that occurs when exposed to ambient air after plasma deposition. When 1 nm of CO was deposited onto 5 nm of CN, an immediate transition from the oxidized layer to the CN layer was observed: the gradient was thus extended to the outermost surface. Note that such result was already obtained when creating an oxygen-containing coating with a lateral chemical gradient: the gradient was also extended to the outermost surface [16]. When 2 or 3 nm of CO was deposited onto 5 nm of CN, a new transition was observed in the evolution of the intensity of oxygen-containing fragments. Indeed, below the oxidized top-layer, a new layer with a higher oxygen-content compared to the CN layer, was detected. In addition, a small transition (at 3 or 4 nm in the depth of coatings CO/CN 2:5 and 3:5, respectively) indicates another layer below this oxygen-containing layer: as a slight decrease of the intensity counts was observed, a lower oxygen-content is expected in this base layer corresponding to the CN layer. Figure 3b reveals that the oxygen content in the CN base layer seems to increase with the CO terminal layer thickness. Actually, the oxygen content should be the same in the bulk of all CN base layers, and this increase is due to the matrix effect, as previously mentioned. This is the reason why the transition in between the CO and CN layers is less sharp, and thus slightly more difficult to observe. Regardless, the position of this transition in the depth clearly depends on the thickness of the CO layer, showing the interface in between CN and CO layers.

Thus, in-depth profiling ToF-SIMS measurements revealed some variation in the chemical composition of the CO layers, depending on the substrate on which this layer was

deposited. Indeed, when the CO layer was deposited onto the CN model surface, a mixture of oxygen- and nitrogen-containing fragments were observed in the top-layer, showing a gradual chemical composition (with a thickness of ~ 4 nm) different from the CO layer deposited onto Si wafer. The formation of such a gradual interface structure was explained by etching and (re-)deposition processes occurring at the same time during plasma deposition of the second layer. Moreover, the CN model surface had the same chemical composition, even after the deposition of the CO layer, but the final film thickness (calculated thanks to the previously determined etching rate) was smaller after CO layer deposition, showing the etching process occurring during the deposition of the CO layer.

In addition, advancing and receding water contact angles are reported in Fig. 4. The CN layer is clearly more hydrophobic than the CO layer, as advancing and receding water contact angle values were at $52 \pm 1°$ and $43 \pm 1°$, respectively. Note that the Si wafer substrate displays a water contact angle of $55 \pm 2°$, which is close to the water contact angle value of the CN coating. The CO terminal coating on top of the CN base film showed similar hydrophilic properties compared to the plain CO layer with 44–45° on average, showing that the deposition of 1 nm of CO top-layer is already sufficient to provide the same WCA values as for the plain CO coating. Lower receding water contact angles were measured for all samples: the CN model surface was slightly less hydrophilic than the CO layer, with $33 \pm 3°$ and $29 \pm 1°$, respectively. CO/CN structures showed again hydration properties close to the CO reference, as a receding angle of $30 \pm 1°$ was measured. Nevertheless, the measured receding contact angle values were found to lie all in a narrow range indicating similar surface processes, mainly water adsorption onto the surface and probably water penetration, regardless of the thickness of the superficial CO layer.

These results were also confirmed by the measurements of the surface zeta potential of the coated surface. As described in the "Methods" section, surface zeta potential was determined by measuring the mobility of dedicated tracer particles at different distances from the surface. Figure 5 shows the surface zeta potential values obtained for the plasma coatings CN, CO, CO/CN 1:5, 2:5, and 3:5. The CN model surface is the least negatively charged ($- 13 \pm 7$ mV) of all coatings investigated. This coating exhibits a surface with primary amine groups ($[NH_2]/[C] \sim 1\%$ [21]) as well as oxygen-containing functional groups ($[O]/[C] \sim 10\%$). Therefore, a mixture of positively and negatively charged functional groups can be expected. For all reference CO and CO/CN coatings, a similar negative surface charging of around $- 48 \pm 2$ mV was obtained, remarkably independent of the thickness of the CO terminal layer. Two conclusions can be drawn from these analyses: (1) the CO surface is electrically equivalent independent of the substrate on which it was deposited, already for a very thin (1 nm) CO termination and (2) the measured surface zeta potential (according to this method) is given for the top 1 nm of the

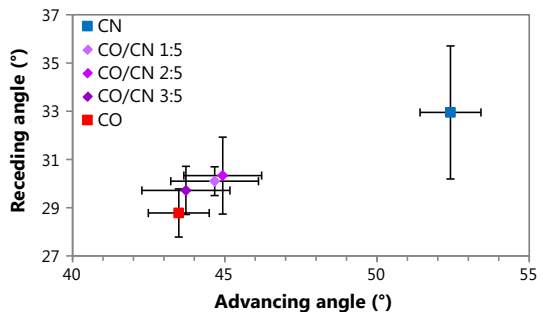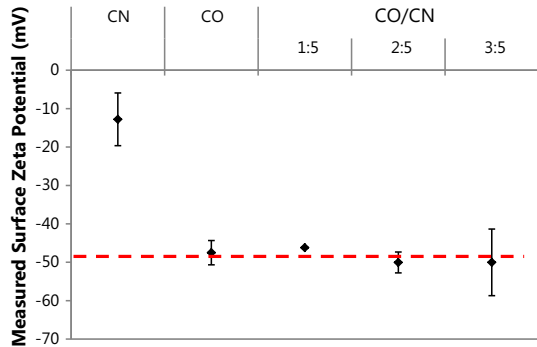**Fig. 4** Dynamic water contact angle values (advancing and receding) for the coatings CO, CN, CO/CN 1:5, 2:5, and 3:5

Fig. 5 Measured surface zeta potential of the coatings CO, CN, and CO/CN (1, 2, and 3 nm) at pH = 7.00 ± 0.05

coatings, as the same surface zeta potential was measured for all the double layer coatings even if the base layer CN may acquire a charge due to water penetration in the coating.

Such analyses on plain and gradient plasma polymer films demonstrated that the surface properties, e.g. wettability and surface charge, were very similar even for a chemical gradient extending to the outermost surface (as for a terminal CO layer thickness close to 1 nm). Since it was already recognized that the single layers and gradient-containing coatings aged according to the same processes in air, yet differently in water [23], it becomes thus interesting to investigate the aging behavior of the CO/CN coatings in water.

Influence of Water Aging on the Chemical Composition of the CO/CN Structures

The chemical and structural stability of ultra-thin plasma polymer films is of high interest that motivated different approaches to reduce aging phenomena over recent years, also including gradient structures [49]. Therefore, static water contact angles were measured after 30 min storage of the PPFs in air or water, and also after 1 day storage in water. Regarding the CN model surface, similar WCA were measured for both storage conditions after 30 min, e.g. a WCA of $55 \pm 3°$ after air storage and of $52 \pm 5°$ after water storage. In addition, after 1 day in water, similar water contact angle values were obtained, e.g. $55 \pm 1°$, indicating the high stability of the CN model surface.

When the CO layer was deposited onto the Si wafer, WCA of $45 \pm 1°$ after air storage and $43 \pm 1°$ after water storage were measured. After 1 day in water, the same coating displayed a WCA value of $46 \pm 2°$, showing the equally high stability of this coating being slightly more hydrophilic than CN. When CO is deposited onto the CN model surface, a WCA of $47 \pm 2°$ was measured after 30 min of storage in air, regardless of the thickness of the top-layer. This value is remarkably similar to the one obtained for the CO reference, e.g. $45 \pm 1°$. After 30 min of storage in distilled water, different WCA values were obtained—this time depending on the thickness of the oxygen-containing termination: for CO/CN 1:5, a WCA value of $51 \pm 2°$ was obtained, which was closer to the WCA value as obtained for the CN coating, indicating that small restructuring and degradation effects of the CO termination layer may have occurred due to hydrolysis of ester groups [16]. When the CO layer had a thickness of 2 or 3 nm, significantly smaller water contact angle values of $41 \pm 2°$ and $44 \pm 1°$, respectively, were measured. These findings are again close to the WCA value obtained for the CO reference, indicating that, even if some chemical changes of the top-layer had occurred, the top-layer largely remained intact over

the immersion time of 30 min in distilled water. After 1 day in water, CO/CN 2:5 and 3:5 displayed WCA values of $41 \pm 3°$ and $43 \pm 2°$, respectively, showing merely minor changes limited to the outermost molecular layer.

The chemical composition in the plasma polymer films was determined by XPS after 1 day in water (Figure S1). The CN model surface is already known to retain its chemical composition when immersed in water over 1 day [21], with [O]/[C] and [N]/[C] ratios of ~ 10 and $\sim 18\%$, respectively. In this study, the chemical composition of the CO layer was also observed to be constant after 1 day in water, with a [O]/[C] ratio of 27.7% (compared to the initial [O]/[C] ratio of 27.9%). When a 1 nm layer of CO is deposited onto the CN model surface, the [O]/[C] ratio was found to be almost similar (25.4% after 1 day in water compared to the initial 26.0%), whereas the [N]/[C] ratio was observed to increase from 5.6 to 9.5%. With the CO termination thickness of 2 or 3 nm minor changes in the chemical composition were observed: for CO/CN 2:5, the [O]/[C] ratio increased from 26.4 to 28.7% and the [N]/[C] ratio slightly increased from 3.3 to 3.8%; and for CO/CN 3:5, the [O]/[C] ratio remained the same with 26.5%, and the [N]/[C] ratio slightly increased from 1.8 to 2.6%. Thus, it can be assumed that some fragments from the CO layer (when deposited onto the CN model surface) were dissolved during water aging which, however, represent less than 1 nm of the CO coating.

To confirm surface degradation effects, evolution of the surface topography was observed by AFM before and after water storage over 1 day (Fig. 6). Note that the RMS roughness of the pristine Si wafer was found to be $S_q = 0.12 \pm 0.03$ nm and the RMS roughness of the CN model surface was found to be $S_q = 0.21 \pm 0.02$ nm. Independent of the substrate surface and the thickness of the CO termination on the CN model surface, similar RMS roughness values were obtained for fresh coatings: S_q (CO) $= 0.17 \pm 0.02$ nm, S_q (CO/CN 1:5) $= 0.18 \pm 0.02$ nm, S_q (CO/CN 2:5) $= 0.18 \pm 0.02$ nm, and S_q (CO/CN 3:5) $= 0.17 \pm 0.01$ nm. After 1 day in water, an increase of the RMS roughness values was observed for all coatings: S_q (CO) $= 0.26 \pm 0.02$ nm, S_q (CO/CN 1:5) $= 0.22 \pm 0.02$ nm, S_q (CO/CN 2:5) $= 0.25 \pm 0.02$ nm and S_q (CO/CN 3:5) $= 0.28 \pm 0.02$ nm. Thus, the AFM results showed a partial dissolution of the CO coating when deposited onto Si wafer or onto the CN model surface and thus an increase in surface roughness at the nanoscale (Fig. 6).

As a conclusion, it was observed based on the change in WCA, the variation of the chemical composition and of the surface topography that the top of the CO layer slightly degraded in water. The release of dissolved fragments seems to occur over 1 day of
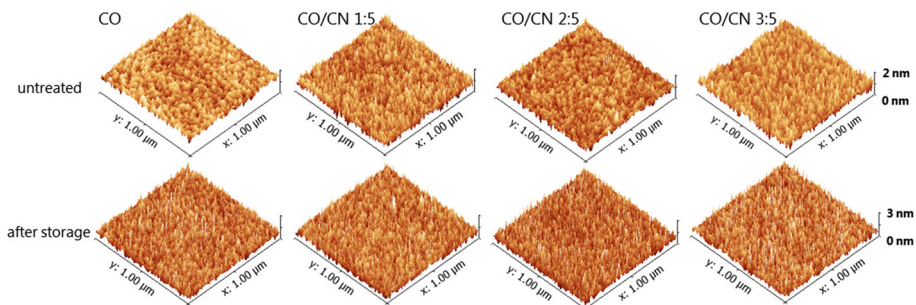

Fig. 6 Topography of the CO layer deposited onto the Si wafer or onto the CN model surface (1, 2, or 3 nm of the CO layer) before and after 1 day water storage as measured by atomic force microscopy (untreated samples: scale from 0 to 2 nm; after storage: scale from 0 to 3 nm)

immersion in water and affects only the top ≤ 1 nm of the coatings, which could be demonstrated by using the adjusted film architectures. The outermost surface of functional PPFs might thus form some low molecular weight organic compounds that can be dissolved [50], which was, however, limited by the design of the CO/CN gradient structure. In accordance, it was recently shown that about 1 nm of a functional CO layer stabilized on a cross-linked CO base layer (termination thickness > 2 nm) can be released when immersed in water for 1 h, while a 1 nm CO termination showed less surface reconstructions [16]. Hence, water interaction with the near-surface structure of the PPFs induced small surface rearrangement effects depending on the exact chemical gradient structure acting as a stabilizing factor. The high cross-linking degree, however, prevented the film from swelling [51].

Protein Characterization and Protein Adsorption onto CO/CN Structures

In addition to the surface characterization of the CO/CN structures as performed in this study, GFP was used as a probe to investigate the surfaces and study their interaction with proteins by monitoring the fluorescence intensity on the differently plasma-coated surfaces. As reported in previous studies on TiO and Pt surfaces [52, 53], GFP was used in this work as a fluorescent probe, as it allowed the direct visualization of adsorbed molecules on the coatings. GFP was selected for its conformational stability and fluorescence properties [54]. To detect the interaction between surfaces and proteins, these are usually labeled with fluorescent dyes that can however alter the global surface potential by involving surface charged residues, and thus the protein adsorption process. Since non-specific adsorption of proteins onto surfaces is affected by surface properties as well as by the physico-chemical properties of the protein itself, the surface potential of the GFP molecule was first analyzed. An equal distribution of regions with positive and negative potential is present on the protein surface (Fig. 7). With an experimentally determined pI of ~ 5 (Figure S2), the GFP molecule carries a net negative charge under the conditions used to study adsorption, e.g. pH = 7. The GFP molecule is monomeric, and presents no extended regions of hydrophobicity on the surface that might promote aggregation (Fig. 7b).

To investigate protein adsorption, the different plasma coatings were incubated for 30 min in a GFP-rich solution (2 mg/mL) and were rinsed three times with distilled water and intermittent air-drying before analysis. The surfaces were imaged with a microarray scanner (resolution = 5–10 μm), and the fluorescence signal was quantified by averaging the fluorescence intensity over nine smaller areas (Figure S3). Note that the intensity of the
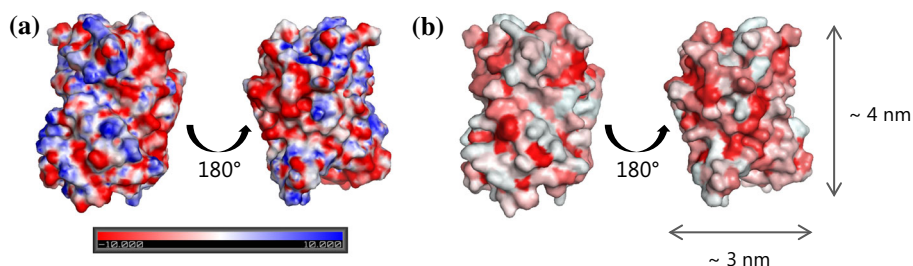

Fig. 7 Surface properties of GFP molecules: a surface electrostatic potential of GFP (blue: positive; red: negative; white: neutral, contour: ± 10 kT/e), and b hydrophobic and hydrophilic areas all around GFP molecules (red: hydrophobic; white hydrophilic) generated using APBS PyMOL visualized on the solvent accessible surface (Color figure online)

fluorescence signal would be affected by denaturation of GFP. In addition, since the drying process is known to have an influence on the protein conformation [55, 56] and thus on the fluorescence intensity, the samples were dried all under the same conditions. The drying process should therefore not have an influence on the relative differences in fluorescence intensity measured between reference and CO/CN structures. Finally, the same washing procedure was applied to all surfaces to remove the loosely bounded GFP, leading to a decrease of the fluorescence signal.

First of all, an increase in the fluorescence of the control surfaces treated with protein-free buffer solution was detected, e.g. intensity values of 6183 and 5121 a.u. were measured for surfaces CN and CO, respectively, whereas values of 5897, 6296 and 7316 a.u. were measured for CO/CN 1:5, 2:5, and 3:5, respectively. These background intensity values were then subtracted from the fluorescence values measured for GFP-treated surfaces in order to determine the fluorescence intensity coming only from the GFP protein (Fig. 8). Note that the overall fluorescence intensities were moderate, since no linkers have been used in order to directly spot the surface properties of the PPFs [57]. Hence, a comparison with literature data regarding the performance of the examined PPFs with respect to high (or low) protein adsorption is complicated. Regardless, it could be observed that the CO/CN coatings resulted in significantly different fluorescence intensities due to adsorbed protein, as compared to the CO and CN coatings used as references (Fig. 8). Furthermore, the subtly different near-surface film structures of CO/CN 1:5, 2:5, and 3:5 revealed remarkable variations in the fluorescence as detected from GFP-treated areas. A significant increase in net fluorescence was observed with the decrease of the CO layer thickness. This finding is surprising, given the similarity of outermost surface chemistry, zeta potential and wettability of the gradient CO/CN films. As previously observed, CO/CN films undergo a partial restructuring of the CO terminal layer in water, enhancing the effect of the sub-surface (i.e. the CN base layer) in the plasma coating/protein interaction. Regardless, the effect of the sub-surface depends on the thickness of the CO top-layer. Thus, this enhanced sub-surface effect may be observed mainly for CO/CN 1:5 and 2:5 films. The near-surface restructuring might yield the exposure of different, also N-containing, functional groups. It can thus be hypothesized that lateral heterogeneities in the nanometer-range occur with which the GFP might interact, while they are not probed by contact angle and surface charge measurements. Accordingly, AFM showed an inhomogeneous degradation of the surface. This assumption is more likely for CO/CN 1:5 films, as the CO top layer was the thinnest. The very low fluorescence obtained for the CO/CN 3:5

Fig. 8 Surface fluorescence of the coatings CN, CO, CO/CN 1:5, 2:5, and 3:5 after incubation in a solution containing GFP. Surface fluorescence was analyzed with a microarray scanner and quantified by image analysis (n = 9, average ± s.e.m.)
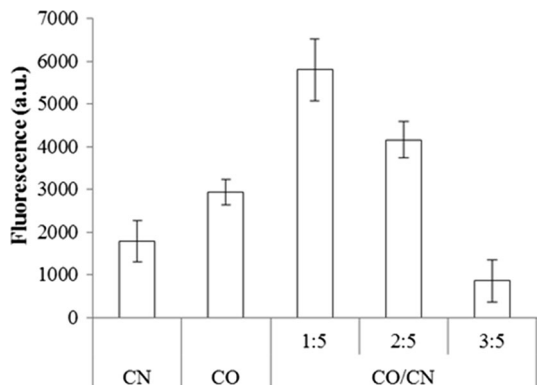
films can also be explained by recent observations made on gradient-containing coatings: the terminal CO layers of increasing thickness were found to exhibit an increasing tendency for motility and reorganization, thus emphasizing the importance of the terminal film thickness and composition [16–18]. The very low GFP adsorption on CO/CN structures with a CO layer thickness $\geq$ 3 nm has also been recognized in a previous study on the micro-patterning of bi-functional PPFs [32, 57].

A similar fluorescence value for all surfaces with similar zeta potential and WCA values (i.e. CO reference and CO/CN gradients) would have been expected, if protein adsorption were solely determined by top surface properties alone. The fluorescence values for the CO/CN samples comprising a near-surface vertical gradient structure, however, were found to noticeably differ from the value obtained for the CO reference, suggesting an influence of the underlying CN layer. As it is well-known, the interaction of proteins such as GFP with surfaces is affected by both surface energy (hydrophobicity) and charge–charge-interactions [58]. It can thus be hypothesized that also a gradient in surface energy and zeta potential extending over a range of a few nanometers of the near-surface structure has a pronounced impact on protein adsorption susceptible to the exact chemical gradient structure. Hence, protein adsorption could be relatively enhanced on such vertical chemical CO/CN nano-gradients with 1–2 nm terminal CO layer.

Conclusion

Nano-scaled oxygen-rich CO layers were deposited onto Si wafer and amine-containing CN model surfaces to investigate the influence of the nature of the substrate and the sub-surface onto the surface properties. The elemental and chemical composition was assessed using XPS and ToF-SIMS techniques. A chemical mixing zone was found forming a vertical chemical nano-gradient between the CO and the CN plasma polymer films. In addition, it was shown that the CO layer deposited onto the CN model surface contained slightly more nitrogen and less oxygen than the CO layer deposited onto the Si wafer also indicating the near-surface chemical gradient structure. Regardless of its thickness, however, the thin CO termination layers showed similar chemical surface composition, wettability, hydration properties and surface charge as the thicker CO reference coating.

After 1 day in water, restructuring and partial degradation of the CO layer was observed, but it was limited to the outermost molecular layers as evidenced on the gradient CO/CN coatings. Accordingly, a higher RMS roughness was detected for all samples. In addition, an increase of the [N]/[C] ratio was observed mainly for the CO/CN 1:5 coating comprising the thinnest termination layer of 1 nm. The actual surface conditions are thus slightly changing in aqueous conditions partly exposing the CN model surface, allowing nitrogen-containing functional groups to be available.

Finally, protein adsorption was observed to be distinctly different for the examined CO surfaces (as deposited onto Si wafer or onto CN base layer) and distinctly depending on the thickness of the top-layer. The green fluorescent protein (GFP) adsorbed in highest amount onto the double layer structure with a 1 nm-thick terminal CO layer, whereas the amount of adsorbed protein was found to be significantly reduced already with a 3 nm-thick top-layer thickness. While it was not the aim to assess the overall performance of the examined PPFs regarding high or low protein adsorption, water interaction and related small surface rearrangements were found to affect molecule-surface interaction such as protein adsorption, which cannot be explained adequately by surface properties alone. Proteins can

thus react sensitively to the structure and composition of plasma polymer films, including the range of a few nanometers below the surface.

References

1. Gunkel G, Huck WTS (2013) Cooperative adsorption of lipoprotein phospholipids, triglycerides, and cholesteryl esters are a key factor in nonspecific adsorption from blood plasma to antifouling polymer surfaces. J Am Chem Soc 135:7047–7052
2. Gunkel G, Weinhart M, Becherer T, Haag R, Huck WTS (2011) Effect of polymer brush architecture on antibiofouling properties. Biomacromol 12:4169–4172
3. Banerjee I, Pangule RC, Kane RS (2011) Antifouling coatings: recent developments in the design of surfaces that prevent fouling by proteins, bacteria, and marine organisms. Adv Mater 23:690–718
4. Tan CK, Blackwood DJ (2003) Corrosion protection by multilayered conducting polymer coatings. Corros Sci 45:545–557
5. Sorensen PA, Kiil S, Dam-Johansen K, Weinell CE (2009) Anticorrosive coatings: a review. J Coat Technol Res 6:135–176
6. Love JC, Estroff LA, Kriebel JK, Nuzzo RG, Whitesides GM (2005) Self-assembled monolayers of thiolates on metals as a form of nanotechnology. Chem Rev 105:1103–1170
7. Makhneva E, Manakov A, Skladal P, Zajickova L (2016) Development of effective QCM biosensors by cyclopropylamine plasma polymerization and antibody immobilization using cross-linking reactions. Surf Coat Technol 290:116–123
8. Altinisik A, Yurdakoc K (2016) Chitosan-/PVA-coated magnetic nanoparticles for Cu (II) ions adsorption. Desalin Water Treat 57:18463–18474
9. Vandenbosche M, Derozier D, Casetta M, Jimenez M, Bellayer S, Traisnel M (2015) An innovative method to functionalize textiles for remediation of polluted media. Appl Surf Sci 330:111–117
10. Jimenez M, Duquesne S, Bourbigot S (2006) Characterization of the performance of an intumescent fire protective coating. Surf Coat Technol 201:979–987
11. Jimenez M, Lesaffre N, Bellayer S, Dupretz R, Vandenbossche M, Duquesne S, Bourbigot S (2015) Novel flame retardant flexible polyurethane foam: plasma induced graft-polymerization of phosphonates. RSC Adv. 5:63853–63865
12. Schlenoff JB (2014) Zwitteration: coating surfaces with zwitterionic functionality to reduce nonspecific adsorption. Langmuir 30:9625–9636
13. Lau KHA, Sileika TS, Park SH, Sousa AML, Burch P, Szleifer I, Messersmith PB (2015) Molecular design of antifouling polymer brushes using sequence-specific peptoids. Adv Mater Interfaces 2:1400225
14. Yasuda H, Matsuzawa Y (2005) Economical advantages of low-pressure plasma polymerization coating. Plasma Process Polym 2:507–512
15. Ligot S, Bousser E, Cossement D, Klemberg-Sapieha J, Viville P, Dubois P, Snyders R (2015) Correlation between mechanical properties and cross-linking degree of ethyl lactate plasma polymer films. Plasma Process Polym 12:508–518
16. Rupper P, Vandenbossche M, Bernard L, Hegemann D, Heuberger M (2017) Composition and stability of plasma polymer films exhibiting vertical chemical gradients. Langmuir 33:2340–2352
17. Hegemann D (2015) Controlling the nanostructure and stability of a-C:H: N plasma polymers. Thin Solid Films 581:2–6
18. Hegemann D, Hanselmann B, Guimond S, Fortunato G, Giraud M-N, Guex AG (2014) Considering the degradation effects of amino-functional plasma polymer coatings for biomedical application. Surf Coat Technol 255:90–95
19. Hegemann D, Körner E, Blanchard NE, Drabik M, Guimond S (2012) Densification of functional plasma polymers by momentum transfer during film growth. Appl Phys Lett 101:211603

20. Hegemann D, Hanselmann B, Blanchard N, Amberg M (2014) Plasma-substrate interaction during plasma deposition on polymers. Contrib Plasma Phys 54:162–169
21. Vandenbossche M, Butron Garcia M-I, Schütz U, Rupper P, Amberg M, Hegemann D (2016) Initial growth of functional plasma polymer nanofilms. Plasma Chem Plasma Process 36:667–677
22. Hegemann D, Lorusso E, Butron Garcia MI, Blanchard NE, Rupper P, Favia P, Heuberger M, Vandenbossche M (2016) Suppression of hydrophobic recovery by plasma polymer films with vertical chemical gradients. Langmuir 32:651–654
23. Dorst J, Vandenbossche M, Amberg M, Bernard L, Rupper P, Weltmann K-D, Fricke K, Hegemann D (2017) Improving the stability of amino-containing plasma polymer films in aqueous environments. Langmuir 33:10736–10744
24. Li L, Dai XJ, Xu HS, Zhao JH, Yang P, Maurdev G, du Plessis J, Lamb PR, Fox BL, Michalski WP (2009) Combined continuous wave and pulsed plasma modes: for more stable interfaces with higher functionality on metal and semiconductor surfaces. Plasma Process Polym 6:615–619
25. Yasuda H (1981) Glow discharge polymerization. J Polym Sci Macromol Rev 16:199–293
26. Spanos CG, Badyal JPS, Goodwin AJ, Merlin PJ (2005) Pulsed plasma chemical deposition of polymeric salt networks. Polymer 46:8908–8912
27. Förch R, Zhang Z, Knoll W (2005) Soft plasma treated surfaces: tailoring of structure and properties for biomaterial applications. Plasma Process Polym 2:351–372
28. Dai XJ, du Plessis J, Kyratzis IL, Maurdev G, Huson MG, Coombs C (2009) Controlled amine functionalization and hydrophilicity of a poly (lactic acid) fabric. Plasma Process Polym 6:490–497
29. Girard-Lauriault P-L, Retzko I, Swaraj S, Matsubayashi N, Gross T, Mix R, Unger WES (2010) Nondestructive sub-surface chemical characterization of air-exposed plasma polymers by energy-resolved XPS. Plasma Process Polym 7:474–481
30. Blanchard NE, Naik VV, Geue T, Kahle O, Hegemann D, Heuberger M (2015) Response of plasma-polymerized hexamethyldisiloxane films to aqueous environments. Langmuir 31:12944–12953
31. Hegemann D, Blanchard NE, Heuberger M (2016) Reduced protein adsorption on plasma polymer films comprising hydrophobic/hydrophilic vertical chemical gradients. Plasma Process Polym 13:494–498
32. Vandenbossche M, Bernard L, Rupper P, Maniura-Weber K, Heuberger M, Faccio G, Hegemann D (2017) Micro-patterned plasma polymer films for bio-sensing. Mater Des 114:123–128
33. Guex AG, Kocher FM, Fortunato G, Körner E, Hegemann D, Carrel TP, Tevaearai HT, Giraud MN (2012) Fine-tuning of substrate architecture and surface chemistry promotes muscle tissue development. Acta Biomater 8:1481–1489
34. Hegemann D, Michlicek M, Blanchard NE, Schütz U, Lohmann D, Vandenbossche M, Zajickova L, Drabik M (2016) Deposition of functional plasma polymers influenced by reactor geometry in capacitively coupled discharges. Plasma Process Polym 13:279–286
35. Moulder F, Stickle WF, Sobol PE, Bomben KD (1995) Handbook of X-ray photoelectron spectroscopy. Physical Electronics Inc., Eden Prairie
36. Korhonen JT, Huhtamäki T, Ikkala O, Ras RHA (2013) Reliable measurement of the receding contact angle. Langmuir 29:3858–3863
37. Corbett JCW, McNeil-Watson F, Jack RO, Howarth M (2012) Measuring surface zeta potential using phase analysis light scattering in a simple dip cell arrangement. Colloid Surf A 396:169–176
38. Zuris JA, Thompson DB, Shu Y, Guilinger JP, Bessen JL, Hu JH, Maeder ML, Joung JK, Chen ZY, Liu DR (2015) Cationic lipid-mediated delivery of proteins enables efficient protein-based genome editing in vitro and in vivo. Nat Biotechnol 33:73–80
39. Heck T, Pham P-H, Hammes F, Thöny-Meyer L, Richter M (2014) Continuous monitoring of enzymatic reactions on surfaces by real-time flow cytometry: sortase a catalyzed protein immobilization as a case study. Bioconjug Chem 25:1492–1500
40. Heck T, Pham P-H, Yerlikaya A, Thöny-Meyer L, Richter M (2014) Sortase A catalyzed reaction pathways: a comparative study with six SrtA variants. Catal Sci Technol 4:2946–2956
41. Faccio G, Senkalla S, Thöny-Meyer L, Richter M (2015) Enzymatic multi-functionalization of microparticles under aqueous neutral conditions. RSC Adv 5:22319–22325
42. Lerner MG, Carlson HA (2006) APBS plugin for pymol. University of Michigan, Ann Arbor
43. Berman HM, Westbrook J, Feng Z, Gilliland G, Bhat TN, Weissig H, Shindyalov IN, Bourne PE (2000) The protein data bank. Nucleic Acids Res 28:235–242
44. Baker NA, Sept D, Joseph S, Holst MJ, McCammon JA (2001) Electrostatics of nanosystems: application to microtubules and the ribosome. Proc Natl Acad Sci USA 98:10037–10041
45. Haïdopoulos M, Horgnies M, Mirabella F, Pireaux JJ (2008) Angle-resolved XPS study of plasma-deposited polystyrene films after oxygen plasma treatment. Plasma Process Polym 5:67–75
46. Fahmy A, Schönhals A, Friedrich J (2013) Reaction of water with (radicals in) plasma polymerized allyl alcohol (and formation of OH-rich polymer layers). J Phys Chem B 117:10603–10611

47. Hegemann D, Hossain M-M (2005) Influence of non-polymerizable gases added during plasma poly-merization. Plasma Process Polym 2:554–562
48. Hegemann D, Körner E, Albrecht K, Schütz U, Guimond S (2010) Growth mechanism of oxygen-containing functional plasma polymers. Plasma Process Polym 7:889–898
49. Vandenbossche M, Hegemann D (2018) Recent approaches to reduce aging phenomena in oxygen- and nitrogen-containing plasma polymer films: An overview. Current Opin Solid State Mater Sci. https://doi.org/10.1016/j.cossms.2018.01.001
50. Poncin-Epaillard F, Brosse JC, Falher T (1999) Reactivity of surface groups formed onto a plasma treated poly(propylene) film. Macromol Chem Phys 200:989–996
51. Zhang Z, Chen Q, Knoll W, Förch R (2003) Effect of aqueous solution on functional plasma poly-merized films. Surf Coat Technol 174–175:588–590
52. Topoglidis E, Cass AEG, Brian O'Regan, Durrant JR (2001) Immobilisation and bioelectrochemistry of proteins on nanoporous TiO_2 and ZnO films. J Electroanal Chem 517:20–27
53. Dreesen L, Humbert C, Sartenaer Y, Caudano Y, Volcke C, Mani AA, Peremans A, Thiry PA (2004) Electronic and molecular properties of an adsorbed protein monolayer probed by two-color sum-frequency generation spectroscopy. Langmuir 20:7201–7207
54. Ward WW (1998) Biochemical and physical properties of green fluorescent protein. In: Chalfie M, Kain S (eds) Green fluorescent protein: properties, applications and protocols. Wiley-Liss, New York, pp 45–75
55. Holtz B, Wang Y, Zhu X-Y, Guo A (2007) Denaturing and refolding of protein molecules on surfaces. Proteomics 7:1771–1774
56. Millqvist-Fureby A, Malmsten M, Bergenstahl B (1999) Spray-drying of trypsin—surface characteri-sation and activity preservation. Int J Pharm 188:243–253
57. Bernard L, Rupper P, Faccio G, Hegemann D, Scholder O, Heuberger M, Maniura-Weber K, Van-denbossche M (2018) Plasma polymer film designs through the eyes of ToF-SIMS. Biointerphases 13:03B417
58. Wahlgren M, Arnebrant T (1991) Protein adsorption to solid surfaces. Trends Biotechnol 9:201–208